2015 IEEE/RSJ International Conference on Intelligent Robots and Systems (IROS)
Congress Center Hamburg
Sept 28 - Oct 2, 2015. Hamburg, Germany

Solar Powered UAV: Design and Experiments

Scott Morton, Ruben D'Sa, and Nikolaos Papanikolopoulos
morto091@umn.edu, ruben@cs.umn.edu, npapas@mail.cs.umn.edu
Department of Computer Science, University of Minnesota

***Abstract*— Unmanned solar powered aircraft offer a unique set of advanced capabilities and have set general aviation records for longest continuous flight and greatest sustained altitude. However, the application of solar powered flight to small scale solar powered unmanned aerial vehicles (UAVs) has seen sparse research activity and is only partially explored. The use of solar power as an energy resource allows small scale UAVs to carry heavier, more powerful sensor payloads, and can extend flight times to over 24 hours, thereby achieving multi-day flight. This work focuses on recent developments by the Center for Distributed Robotics on a four meter wingspan solar UAV designed for low altitude aerial sensing applications. Highlighted in this paper are aspects of airframe, propulsion, and electronics hardware design as well as experiments that quantify the solar power system and airframe performance.**

I. INTRODUCTION

Over the past decade, interest in unmanned aerial vehicles (UAVs) has rapidly expanded with research efforts spanning commercial, industrial, and governmental domains. Commercially, UAVs have demonstrated uses in package delivery, cinematography, security, journalism, and news reporting. In industrial production settings, UAVs have shown uses for large structure or machine inspection, construction monitoring and documentation, and perhaps most significantly, precision agriculture. Regarding government entities, the military has long used UAVs for a wide variety of missions. Law enforcement has more recently begun using UAVs in criminal investigations, and surveillance. Additionally, UAVs have shown strong potential for search and rescue missions, forest fire detection and monitoring, weather measurement and forecasting, and disaster relief. The potential uses, in general, are very diverse and as UAV technology becomes more accessible, UAVs will continue to be used in new and surprising ways. At this point the value and usefulness of a mobile aerial platform is beyond doubt. The questions that remain in UAV research are focused on the extent to which UAVs will enter everyday life and what tasks they will be capable of performing.

Aerial robotics platforms can be classified into fixed wing and rotorcraft variants. Rotorcraft achieve flight through lift generated by rotating airfoil shaped blades, while fixed wing aircraft primarily generate lift from airflow over wings. Generally, rotorcraft are more maneuverable and precise due to the ability to hover in place. Fixed wing aircraft fly more efficiently, and have greater payload capacity, range, altitude and endurance characteristics. Hybrids, that successfully combine various aspects of both aircraft types have also been demonstrated.

An active research area in fixed wing UAVs is the use

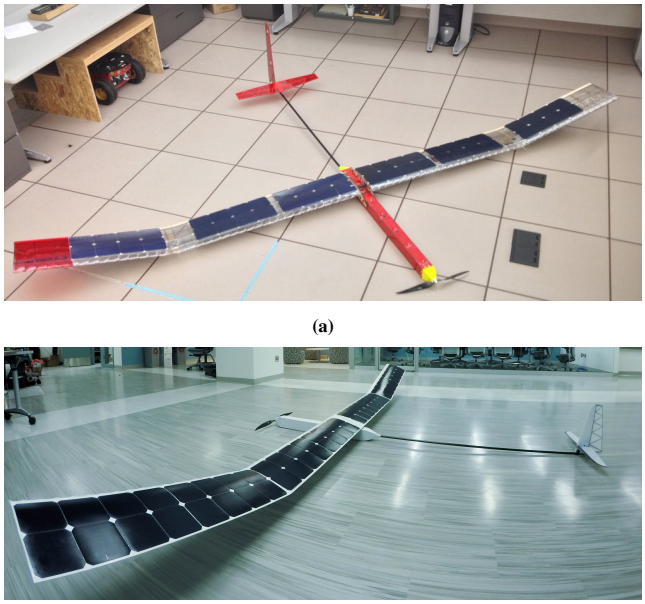

(a)

(b)

Fig. 1: Version 1.0 (a) and 1.1 (b) solar UAV prototypes developed at the Center for Distributed Robotics. Version 1.0 has a maximum solar power capacity of 145 watts while version 1.1 is is capable of 180 watts. Each has a wingspan of 4 meters.

of solar power as an energy resource. The physics of solar powered flight are such that it is possible for significantly more solar power can be captured on an aircraft's surfaces than what is required for flight. The surplus of power is therefore available to propel the aircraft, power payload electronics, or store in batteries. If more solar energy is stored than what is required to fly through the night, multiple-day continuous flight is possible.

A number of documented solar powered flight attempts have been made since the inceptive flight on November 4, 1974 [1]. Since then, manned and unmanned solar powered aircraft have been developed. The first piloted solar powered aircraft was developed by the AeroVironmnent company and took flight on May 18, 1980 [2]. Notable unmanned aircraft include the NASA Pathfinder [3] and Helios [4], and the Zephyr aircraft developed by Qinetiq Inc. [5]. Each of these set new records for solar powered aircraft and aviation in general. The NASA Helios reached an altitude of over 96,000 feet, which was a world record for steady state horizontal flight by a winged aircraft. The Qinetiq Zephyr set a world record for the longest continuous flight by staying aloft for over two weeks. Both of these aircraft demonstrate the advanced capabilities solar powered aircraft, however, these were large aircraft that required a runway for takeoff.

The first documented multi-day flight of a small scale solar

UAV was the SoLong by Alan Cocconi. The aircraft had a 4.75m wingspan and achieved 48 hour flight from June 1-3, 2005. This proved that continuous flight is possible at small scale, however, it weighed over 12kg and required a runway for takeoff. A more practical documented experimental work is that of A. Noth [6], [7], [8], [9]. The aircraft was 3.2 meters in wingspan, completed a 27 hour flight, and was capable of hand launched takeoff. Other theoretical works have considered control and path planning for different solar aircraft missions [10] and optimization for continuous flight [11], [12].

As will be discussed in Section IV, the solar UAV version 1.1 prototype presented in this work has a 4 meter wing span and is capable of a maximum of 180 watts of solar power. This is in contrast to the work by A. Noth which had a wing span of 3.2 meters and a solar power capability of 90 watts. The power requirement of the version 1.1 prototype was found to be less than 46.8 watts during level flight allowing the aircraft to achieve a greater maximum power margin, and therefore power significantly more demanding payloads during solar flight. Additionally, increased airframe size and available solar power provides a more versatile infrastructure for on-board sensors, wireless communication, and computational hardware as highlighted in Section III-C. Methods used to design the airframe, propulsion, and electronics of the solar UAV prototype are presented in Sections II-A, II-B, and II-C, respectively. A description of the solar UAV 1.1 is provided in Section III.

II. Solar UAV Design Methods

A. Airframe Design

The design objective of an airframe for small solar UAVs is to optimize the aircraft for efficient flight while meeting the other necessary flight and sensory requirements. For the design objectives of low altitude data collection, important additional considerations include payload capacity, controllability, and hand launched takeoff. Level flight power describes the condition where the aircraft is operating at steady state with minimal power consumption. This is assumed to be the primary state for solar powered flight and is therefore, the condition for which the airframe should be optimized for efficiency. The level flight power derivation is summarized in previous work [12], but is repeated here for convenience:

$$P_{level} = F_D V = C_{D_\alpha} C_{L_\alpha}^{-\frac{3}{2}} W^{\frac{3}{2}} \frac{\rho S}{2}^{-\frac{1}{2}}. \quad (1)$$

Where C_{L_α} and C_{D_α} are the aircraft lift and drag coefficients, ρ is the air density, S is the wing reference area, and V is the airspeed. For the primary objective of efficient flight, airfoil and wing geometry are two of the most important design choices. The airfoil defines the lift and drag characteristics of the wing and should be designed or selected such that level flight power is minimized. However, the airfoil shape also determines the surface of the solar array. Airfoils with greater curvature may be more efficient, but may also be unsuitable for solar cells that have limited flexibility. Wing geometry also has dramatic implications in terms of flight efficiency and power output from the solar array. Generally for minimal drag, high aspect ratio wings are optimal [13]. This can be verified through a lifting line analysis [14], which takes into consideration the varying induced angle of attack across the wing to determine the overall C_D and $C_L^{-3/2}$. A graph of $C_{D_\alpha} C_{L_\alpha}^{-3/2}$ versus aspect ratio as determined through lifting line analysis is shown in Figure 2. This clearly shows the negative relationship between level flight power and aspect ratio with all else is held constant.

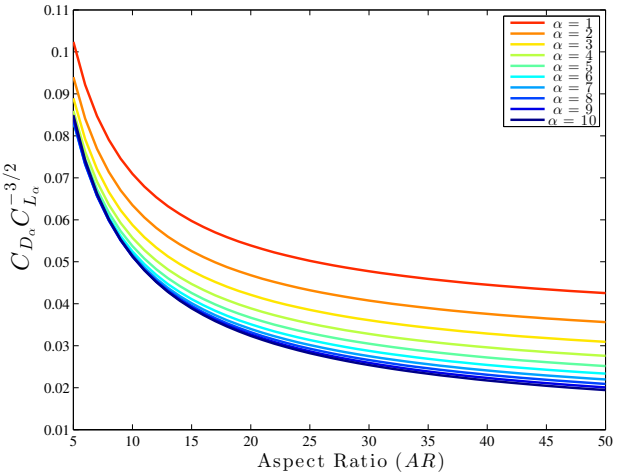

Fig. 2: This figure displays the relationship between aspect ratio and level flight power in terms of the coefficient of lift and drag as predicted by the lifting line model. Parameters based on the Eppler e210 airfoil of the solar UAV prototype 1.1 were used. These include zero lift angle of attack of -5.0 degrees and a 2D lift coefficient slope of 2π $Nm^{-1} radians$. α is the angle of attack of the wing.

Setting aside the fact that higher aspect ratio wings result in a more efficient airframe, it is worthwhile to investigate how enlarging the wing affects overall solar UAV performance based on a level flight power analysis. One of the important performance metrics for solar powered flight is the ratio of solar power production to level flight power consumption. As shown in [12], the captured solar power P_{solar} is approximately proportional to S assuming the wing reference area is equal to the area of the solar array (the solar array covers the entire wing reference area). Incorporating the relationship of S to P_{level} in Equation (1), it can be observed that:

$$P_{solar} \propto S, \quad (2)$$

$$\frac{P_{solar}}{P_{level}} \propto S^{\frac{3}{2}}. \quad (3)$$

Factors that limit wing length include the associated additional weight, and the load bearing capacity of the wing structure. Additional wing length may be prohibitive because it adds weight both directly and indirectly through the additional structural support required at the wing root. In terms of structural limitations, it may not be possible for the structure required to fit within the wing cross section without significantly adding complexity to the airframe. Therefore

wing length must be analyzed by considering weight and structural factors in addition to solar power capacity.

Fabrication of the airframe must consider the properties of materials used and the availability of components. Such components include the electric motor, gearbox, high modulus pultruded carbon fiber, solar modules, and battery cells. These components must be optimized based on the discrete options available which may have limited manufacturing specifications and tolerances. Uncertainties in these components lead to deviations from the models used during optimization. Therefore, to validate the optimization methods, empirical investigations must be performed.

To be flyable, an aircraft must meet a set of stability requirements. The goal of designing for stability is to produce an airframe that when perturbed, generates the aerodynamic forces necessary to return the aircraft to the initial state. Aircraft stability and control feature several trade offs in terms optimizing solar powered aircraft design. For example, a larger tail stabilizer provides better yaw and pitch stability, however, this will contribute to weight and skin friction drag. The dihedral (wing angle with respect to the horizontal plane), improves roll stability during flight maneuvers. However, a larger dihedral reduces level flight efficiency since a portion of the lift generated is directed inward. Moreover, it would also cause the solar array to be positioned at a greater average angle of incidence with respect to the sun during level flight, thereby reducing its output. In terms of control, the number of control surfaces can be reduced by excluding ailerons, and enlarging the rudder surface area to control roll through the dihedral effect. However, this configuration is at the expense of maneuverability and roll responsiveness in rough weather conditions when compared to including ailerons.

B. Propulsion

The propulsion system converts electrical energy into kinetic energy through the serially connected chain of the controller, motor, (gearbox), and propeller. Propulsion system design for an endurance focused solar aircraft differs from that of a typical aircraft in several ways. A solar powered aircraft will spend the vast majority of its flight time in level flight in order to minimize power consumption, therefore the propulsion group should be optimized to maximize efficiency at these conditions. A propeller and motor each have a single operating point of peak efficiency. Therefore, the key to maximizing the overall efficiency is aligning these points at the aircraft level flight condition. Propellers operate most efficiently when no part is stalled and when turbulence losses are at a minimum. This generally prescribes a large propeller that operates at relatively low angular velocity and high torque. Electric motors, however, are generally more efficient and compact when designed for low torque and high angular velocity. Thus, there is a trade-off between using a less efficient direct drive motor and a higher efficiency motor that requires a gearbox with inefficiencies and susceptibility to wear. The motor and propeller pair must also be capable of providing the thrust required for takeoff, as this is the most power demanding period during a mission optimized for high endurance.

Commercially produced propellers that are large diameter (greater than 50cm) and folding are very few in number. Small scale solar aircraft use folding propellers to reduce the complexity and/or drag associated with landing gear. Without landing gear, a front mounted propeller must fold for landing. Propellers can be designed specifically to meet solar UAV flight conditions and produced with carbon fiber in a mold. For a particular propeller, an empirical fit can be established through wind tunnel testing as shown in Figure 4. The data was collected in the 101.6x127.0 cm cross section closed return wind tunnel in the aerospace department at the University of Minnesota. Measurements of thrust were taken using a 6 degree-of-freedom sting and airspeed measurements were collected using a pitot static tube mounted upstream of the propeller. Correction factors for propeller testing are described by Brandt and Selig [15]. The motor efficiency was estimated using torque measurements from the sting, angular velocity from an Extech RPM10 infrared tachometer, and electronic speed controller voltage and current from Agilent U1253A digital multimeter.

The strategy implemented to select the motor and gearbox was to search model aircraft motor data. Data on over 4100 motors were collected. The motor selection was conducted through a search for maximum efficiency at the level flight condition with varying gear ratios, while also meeting the takeoff power requirements. The maximum efficiency was computed by prescribing the torque and angular velocity requirements of the propeller at level flight conditions. The gear ratio N forms a relationship between the motor torque Q_m and angular velocity Ω_m such that $Q_m N = Q_{out}$ and $\Omega_m / N = \Omega_{out}$, therefore the level flight condition determines a relationship between Q_m and Ω_m:

$$Q_m \Omega_m = \frac{Q_{out} \Omega_{out}}{\eta_{gb}}, \tag{4}$$

where η_{gb} is the efficiency of the gearbox. This value can be estimated based on the type of gearbox used, such as planetary, pinion and spur gear, or multistage pinion and spur gear. Further, it can be varied as a function of any of the associated power transfer parameters.

The efficiency of a direct current motor is estimated through the following relationship:

$$\eta_m = \left[1 - \frac{i_0 R}{v - \Omega_m / K_v} \right] \frac{\Omega_m}{v K_v}, \tag{5}$$

where motor parameters are described by the no load current i_0, the motor speed constant K_v, and the motor coil resistance R. Using these parameters, the back-EMF of the motor v can determined by the following equation:

$$v = R(Q_m K_v + i_0) + \frac{\Omega_m}{K_v}, \tag{6}$$

This is allowed to vary since the effective voltage is governed by motor controller's duty ratio through pulse width modulation. In addition, the battery voltage can be

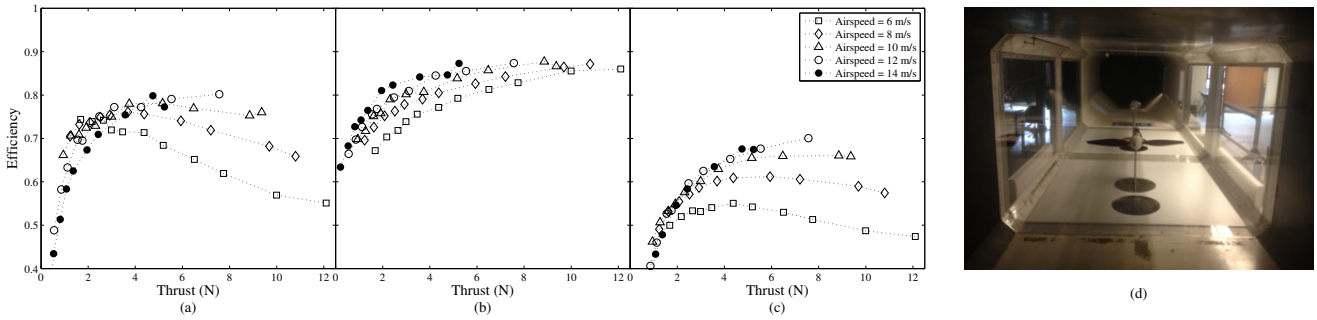

Fig. 3: This figure displays experimental wind tunnel efficiency measurements of a propulsion system composed of a 58.42x30.48 cm RFM propeller paired with 2.5° of pitch and an AMMO 1530kv inrunner motor with a 4.3 gear ratio planetary gearbox. The plots display the estimated efficiency of the (a) propeller, (b) motor, gearbox, and speed controller, and (c) combined system at different thrust levels and wind tunnel airspeeds. This demonstrates the approach used to validate propulsion components and estimate in flight performance. (d) displays the experimental setup looking downwind toward the sting.

assumed to be dependent on requirements of the propulsion system. The relationship between voltage, Q_m and Ω_m can by modeled to the first order [16] by the following equation:

$$Q_m = \left[\left(v - \frac{\Omega_m}{K_v}\right)\frac{1}{R} - i_0\right]\frac{1}{K_v}. \tag{7}$$

Therefore, for the Q_{out} and Ω_{out} of the propeller at level flight conditions, the maximum efficiency of the motor for all gear ratios can be estimated.

According to the aforementioned relationships, the theoretical maximum power and maximum efficiency solution sets for the surveyed motors were computed as shown in Figure 4 (b). This plot shows the high variance in efficiencies, however, it can be observed that generally greater maximum efficiency is possible at greater motor mass. Greater mass increases level flight power with a power of 3/2 as shown in Equation (1), illustrating the tradeoff between mass and efficiency. For hand launched takeoff in no wind, the airspeed $V_{\infty,to}$ can be assumed to be $4ms^{-1}$. The wing should have an angle attack that maximizes lift, but is conservatively far away from stall. The propulsive thrust must overcome drag as well as make up for any lifting force required which the wing cannot produce at the takeoff airspeed.

Figure 4 (c) displays the geared solution set for a select group of motors considered for level flight propeller requirements of 0.3 Nm and 2000rpm. From this plot it can be seen that several motors have a maximum efficiency that is near the propeller prescribed conditions, meaning no gearbox would be required. However, these direct driver motors may be more inefficient than higher rpm motors even after the added inefficiency of a gearbox. The motor weight must also be appropriately analyzed against efficiency gains since the additional propulsive power required to lift a heavier but more efficient motor may overcome the power saved through better efficiency. Additionally, other characteristics such as form factor, aerodynamics, and maintenance must be considered.

C. Power Electronics and Solar Array

The overall design objective of the power electronics is to manage power transfer with reliability, high power-converter efficiency, and to minimize the weight of the components used. The power electronics components include the solar array, maximum power point tracker, battery protection circuit, and the motor controller. The type of solar cells selected has one of the most significant impacts on the overall flight time performance. In selecting solar cells, the significant specifications are nominal efficiency, nominal voltage per cell, maximum current handling, efficiency degradation with temperature, and wavelength response. Maximum efficiency of the solar cells determines the maximum total output of the solar array and is the most significant criterion when evaluating solar cell options. The nominal voltage per cell along with the number of cells defines the nominal total voltage of the solar array since in a single array all solar cells are connected in series. The total voltage of the solar array has significant implications for the transfer of power from the solar array to the battery or motor controller. With a single array, if the voltage of the array is less than what is required to charge the battery and power the motor controller, more complex voltage boosting power electronics will be required. To maximize the efficiency of the solar array, a maximum power point tracker (MPPT) is used. A MPPT actively controls the output voltage of the solar array such that the power output is maximized. For aircraft that have solar arrays located on surfaces with varied angles, it is ideal for each array to be on an individual MPPT circuit. This is because arrays on different surfaces will experience different levels of solar irradience since they capture different cross sections of solar radiation. This in turn causes the solar arrays to operate at a different location on their voltage-current curve. From the output of the MPPT, power conversion circuitry is required to provide a constant regulated voltage source to the battery and motor controller. In terms optimal battery type for solar powered aircraft, those with the highest energy density at an economical cost are lithium based. These batteries feature a number of isolated cells that can become unbalanced after charging and discharging. Unbalanced cells can lead to overcharging and reduced life, therefore battery protection and balancing electronics are required.

For a given solar array, the solar power captured is dependent on the alignment of the solar array to solar radiation and present weather conditions. Alignment is dependent on the aircraft yaw, pitch and roll, solar array configuration on the aircraft, and relative location of the sun in the sky. The

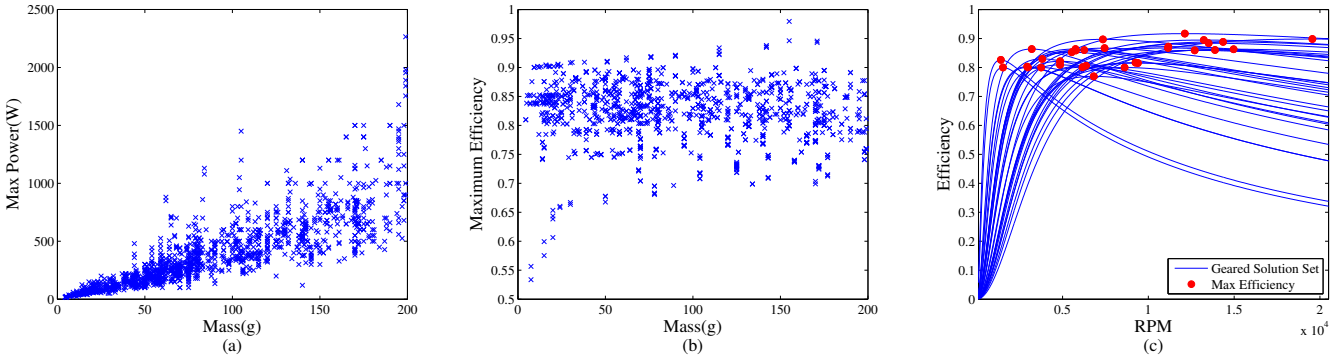

Fig. 4: Maximum power (a) and efficiency plots (b) of surveyed model aircraft motors. (c) Estimated efficiency for selected motors with varying gear ratios for a propeller torque of 0.3 Nm and angular velocity of 2000 rpm as prescribed by propeller data at level flight condition. Motors were selected based on ability to meet takeoff requirements and a minimum max efficiency of 75%.

location of the sun is determined by the time of day, time of year, and geographical location. During winter months, the sun has a more shallow trajectory in the sky resulting in less overall capability to capture solar power during level flight.

III. Solar UAV Prototype

A. Airframe and Propulsion

Shown in Figure 1 are the versions 1.0 and 1.1 solar UAV prototypes developed at the CDR. Version 1.1 has a number of improvements to performance across several metrics. In terms of weight, it is significantly reduced by storing batteries and electronics in the fuselage, decreasing the tail size, using lighter materials, and switching from a heavier direct drive out-runner motor to a high efficiency geared in-runner. Control authority is improved by moving the tail further from the center of gravity while maintaining control surface area.

TABLE I: Mass of solar UAV prototype components

Component	v1.0	v1.1 (g)
Solar Cells	860	790
Fuselage	1150	840
Wing	895	1200
Propulsion	434	325
Total	3663	3155

The wingspan of both versions is 4 meters, which was chosen as a balance between portability and payload capacity. The airframe structure is primarily basswood, pultruded carbon fiber, polypropylene sheet, ABS plastic and nylon fasteners. The dihedral of the wing is set at 14.25 degrees with a length of 1.14 m. The wing structure consists of carbon fiber tubing, carbon fiber stringers, basswood ribs and an encapsulant wrap as shown in Figure . The central spar is a 1.65 cm outer diameter unidirectional carbon fiber tube with a wall thickness of 0.12 cm and a manufacture stated tensile modulus of approximately 80 GPa. The basswood ribs are 0.16 cm thick and pultruded carbon fiber stringers are 0.53 mm x 2.8 mm with a stated tensile modulus of 135 GPa. A polypropylene wrap encapsulates the ribs, forming outer shape of the wing. The unidirectional rod and stringers provide the majority of the structural support for the wing. The high tensile modulus carbon fiber stringers are designed to provide bending rigidity while the carbon fiber tube maintains the wing geometry. The wing profile is constant from root to tip and uses the SD5060 airfoil with a 30.5 cm chord length for version 1.0 and an Eppler e210 for version 1.1. The SD5060 airfoil was chosen for its low curvature on the upper surface of the airfoil since this was the location for mounting solar cells. However, a thinner encapsulant used for version 1.1 allowed for more solar array flexibility and therefore a greater airfoil curvature. This in turn allowed for the more efficient (reduced resulting $C_{D_\alpha}/C_{L_\alpha}^{\frac{3}{2}}$) Eppler e210 airfoil to be used.

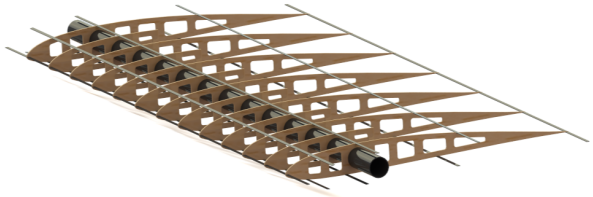

Fig. 6: This figure is a wing structure model developed for the prototype solar UAV. High modulus pultruded carbon fiber stringers are located at the perimeter of the wing to increase bending rigidity and maintain the airfoil cross section between the tibs. The center spar is a filament wound carbon fiber tube which provides torsional rigidity and is the primary structural component of the wing.

B. Power Conversion and Electrical Hardware

Shown in Figure 7 is the version 1.1 electrical topology. The solar array of the prototype consists of 64 Sunpower C-60 cells separated into four arrays, one for each section of the wing. A sectioned approach was used to minimize the losses associated with the dihedrals discussed in Section II-C. A total of 36 Panasonic 18650b cells are used in a 6s6p configuration. The fully charged voltage is 25.2V with a total capacity of 452Wh. To prevent the overcharging of cells during the charging process, a separate protection circuit board is used. A custom designed MPPT using a 4 phase interleaved DC-DC boost topology was designed, prototyped, and validated in section IV. By interleaving multiple phases and leveraging a high switching frequency, it's possible to achieve high converter efficiency with small mass.

C. Sensing and Processing

To process sensor information, version 1.1 utilizes a variety of computational platforms as outlined in Figure 5. The

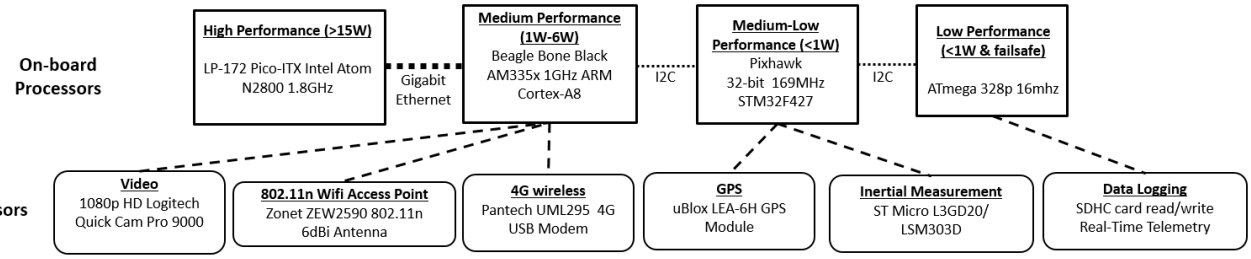

Fig. 5: All on-board processors and the sensors they interface with. The processors share a data connection with one another allowing for computational performance boosts through data offloading.

Beagle Bone Black acts as the central hub for wireless and video processing. It has the capability of interfacing with a variety of sensors while drawing a minimal amount of power. A Logitech Quick Cam Pro 9000 is connected to a Beagle Bone Black to provide low power consumption video streaming. In addition to the camera, a Zonet ZEW2590 802.11n wireless card with a 5 dBi duck antenna is connected over USB. Running Debian, the Beagle Bone Black is setup as a wireless access point to stream video from the Logitech camera and act as the central hub for transferring data to an Intel Atom N2800 over gigabit ethernet for processing. In addition to streaming video, the wireless access point of the Beagle Bone Black allows for distributed communication across ground and aerial systems. Bridged with the on-board Pantech UML295 4G USB modem, telemetry is possible whenever in range of cellular network infrastructure.

A Pixhawk autopilot from 3D Robotics is used for controlling both manual and autonomous flight states. The Pixhawk features flight logging, GPS, roll, pitch and yaw headings, velocities and accelerations and airspeed measurements. Inertial measurement is provided by the Pixhawk's on-board ST Micro L3GD20 3-axis 16-bit gyroscope, ST Micro LSM303D 3-axis 14-bit accelerometer/magnetometer and Invensense MPU 6000 3-axis accelerometer/gyroscope. System parameters are sent from the Pixhawk via a 915 Mhz XBee module equipped with a 2 dBi duck antenna on both the transmitting and receiving end. At its maximum power operation of 50 mW, the XBee has an outdoor line of sight communication range of 6 miles. Atomospheric pressure is measured by an MEAS MS5611 barometer. To sense air speed, a Measurement Specialties 4525DO air speed sensor is connected to the Pixhawk over SPI.

The weight distribution across the component groups is shown in Table I. From the weight proportions, it is evident that the solar cells, fuselage and wing make up the majority of the aircraft weight. The weight of the solar array is primarily govern by the encapsulation materials. The Sunpower C-60 solar cell weight is stated to weigh approximately 1.5g resulting in a total cell weight of approximately 72g. This accounts for less than 10% of the total solar array mass.

IV. Experimental Tests

A piloted test flight of solar UAV version 1.1 was performed on February 12, 2015 with an ambient temperature of -3°F. Figure 8 displays the power draw of the propulsion system during takeoff and level flight. During takeoff and ascent, significantly greater power draw is required as illustrated during the first 15 seconds of flight. The second half of the flight consists of conditions that more closely resemble level flight. Average power consumption during the first 15 seconds of takeoff is 127.32 watts which drops to an average of 43.26 watts during the remainder of the flight. It is speculated that this is a rather conservative estimate of level flight performance since optimized level flight would have consistent and minimized power usage.

Figure 9 displays an experiment consisting of the version 1.1 MPPT with 64 Sunpower C-60 solar cells mounted on a ground test platform. An adjustable power resistor was used as a resistive load and connected to the output of the MPPT. The resistance was set such that the MPPT would not saturate maximum output voltage (25.2V) allowing for maximum solar power to be measured. The entire array was mounted on an adjustable platforms and angled to 80° with respect to ground. Test data was acquired at 1300 hours central time on January 30, 2015 at 44°5822.785N, 93°144.75W with a 8°F solar cell temperature. The average solar power was 146.69 watts. Although the array is designed to output

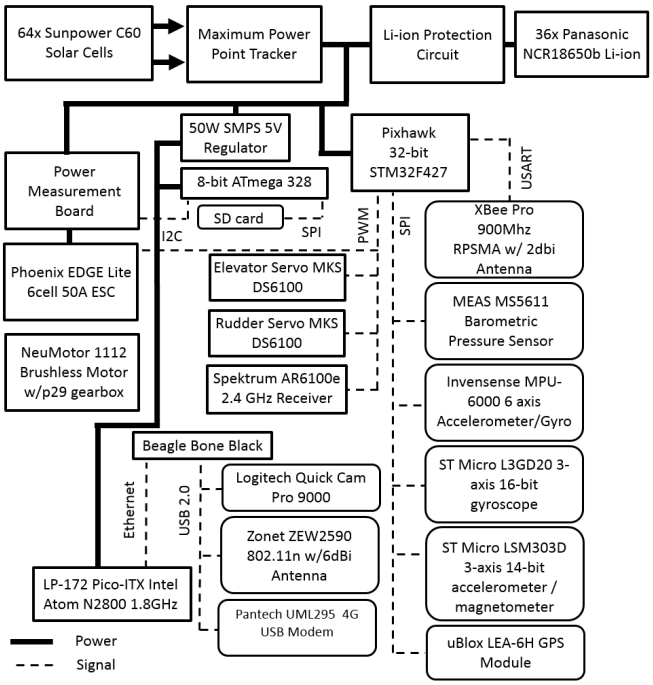

Fig. 7: The electrical topology of version 1.0 solar UAV prototype. This figure illustrates the relationship between the embedded processing, propulsion, and power electronic components.

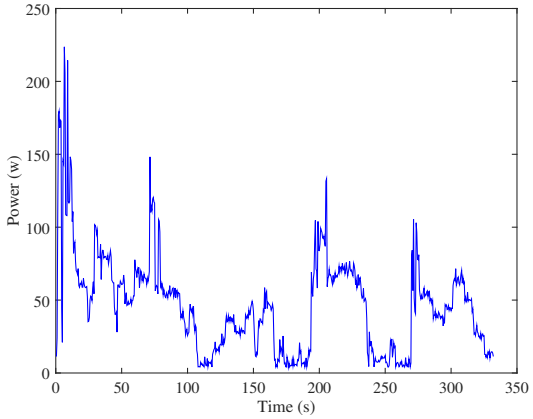

Fig. 8: Flight performance of version 1.1 airframe on Feb. 12, 2015. Including the takeoff power, level flight power averaged 46.8 watts. High windspeeds and teleoperated control resulted in high variability in throttle and power consumption.

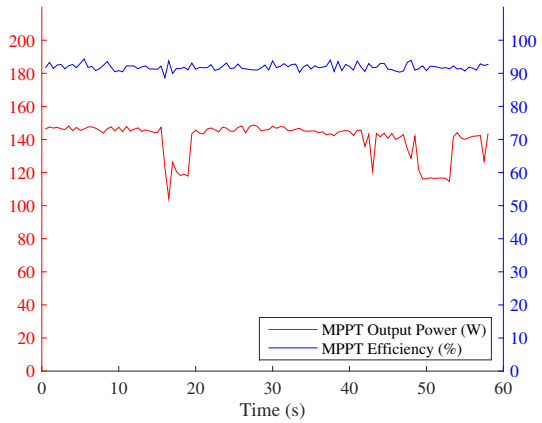

Fig. 9: Version 1.1 ground testing of solar array consisting of 64 Sunpower C-60 cells tested on Jan. 30, 2015.

180 watts under ideal solar conditions, losses in the power electronics, and non-ideal solar conditions resulted in a less than maximum theoretical power output.

An important characteristic for the power electronics is the MPPT's response to variation in solar irradiance. Depending on flight plan objectives, the solar UAV may make roll, pitch, and yaw movements. Changes about these axes can cause the angle of solar irradiance to change resulting in a variation in maximum available solar power. Variation in power can also result from shadows on the solar array as demonstrated by the reduction of MPPT output power in Figure 9. Despite these disturbances, the MPPT maintains an average efficiency of 91.59% with a peak efficiency of 94.33% validating the maximum power point tracking performance in variable solar array conditions.

V. Conclusions

In this work, design considerations associated with solar powered UAVs are presented, a prototype small scale solar UAV is described, and validation of the prototype is demonstrated through several experimental tests. The experiments show that captured solar power accounts for over 300% of a conservative estimate of the power required for level flight. Although this work adds to the few experimental efforts for developing solar powered aircraft, significant theoretical and experimental work remains before a mature understanding and accurate modeling of small scale solar powered UAVs is developed. Specifically, an investigation into smaller scales is warranted since many factors associated with scaling such as aerodynamic efficiency, realizable aircraft weight, and maximum theoretical flight time are not well understood in the context of optimizing solar UAV design. Future work with the solar UAV prototype will be focused on experimental measurements of maximum flight endurance in various flight conditions. In addition, studies into optimal path planning and control of solar UAVs appear to be promising research topics to further enhance solar UAV performance.

VI. Acknowledgements

This material is based upon work supported by the National Science Foundation through grants IIP-0934413, IIS-1017344, CNS-1061489, IIS-1427014, IIP-1432957, and CNS-1531330. Ruben D'Sa was supported by a National Science Foundation Graduate Research Fellowship No. 00039202.

References

[1] R. Boucher, "Sunrise, the world's first solar-powered airplane," *Journal of Aircraft*, vol. 22, no. 10, pp. 840–846, 1985.
[2] P. MacCready, P. Lissaman, W. Morgan, and J. Burke, "Sun-powered aircraft designs," *Journal of Aircraft*, vol. 20, no. 6, pp. 487–493, 1983.
[3] K. Flittie and B. Curtin, "Pathfinder solar-powered aircraft flight performance," vol. 4446. AIAA, 1998.
[4] T. Noll, J. Brown, M. Perez-Davis, S. Ishmael, G. Tiffany, and M. Gaier, "Investigation of the Helios prototype aircraft mishap report, NASA," 2004.
[5] J. Amos, "'Eternal plane' returns to Earth. BBC News, 2010. "http://www.bbc.co.uk/news/science-environment-10733998."
[6] A. Noth, W. Engel, and R. Siegwart, "Design of an ultra-lightweight autonomous solar airplane for continuous flight," *Field and Service Robotics*, vol. 25, pp. 441–452, 2006.
[7] A. Noth, M. Engel, and R. Siegwart, "Flying solo and solar to Mars," *IEEE International Conference on Robotics and Automation*, vol. 13, no. 3, pp. 44–52, 2006.
[8] A. Noth, R. Siegwart, and W. Engel, "Autonomous solar UAV for sustainable flights," in *Advances in Unmanned Aerial Vehicles*, ser. Intelligent Systems, Control and Automation: Science and Engineering. Springer Netherlands, 2007, vol. 33, pp. 377–405.
[9] A. Noth, "Design of solar powered airplanes for continuous flight," Ph.D. dissertation, Autonomous Systems Lab, ETH Zurich, 2008.
[10] A. T. Klesh and P. T. Kabamba, "Solar-powered aircraft: Energy-optimal path planning and perpetual endurance," *Journal of guidance, control, and dynamics*, vol. 32, no. 4, pp. 1320–1329, 2009.
[11] S. Leutenegger, M. Jabas, and R. Siegwart, "Solar airplane conceptual design and performance estimation," *Journal of Intelligent Robotic Systems*, vol. 61, no. 1-4, pp. 545–561, 2011. [Online]. Available: http://dx.doi.org/10.1007/s10846-010-9484-x
[12] S. Morton, L. Scharber, and N. Papanikolopoulos, "Solar powered unmanned aerial vehicle for continuous flight: Conceptual overview and optimization," in *Proceedings of the IEEE International Conference on Robotics and Automation*, 2013, pp. 766–771.
[13] D. P. Raymer *et al.*, *Aircraft design: a conceptual approach*. AIAA, 1999, vol. 3.
[14] M. Drela, *Flight Vehicle Aerodynamics*. MIT Press, 2014.
[15] J. B. Brandt and M. S. Selig, "Propeller performance data at low reynolds numbers," in *49th AIAA Aerospace Sciences Meeting*, 2011, pp. 2011–1255.
[16] M. Drela, *DC Motor / Propeller Matching Course Notes*. MIT Press, 2005.